Article

Reduction of Oxidizable Pollutants in Waste Water from the Wadi El Bey River Basin Using Magnetic Nanoparticles as Removal Agents

Hajer Tlili [1,2], Anis Elaoud [2,3], Nedra Asses [2], Karima Horchani-Naifer [1], Mounir Ferhi [1], Gerardo F. Goya [4,5] and Jesús Antonio Fuentes-García [4,5,*]

[1] Laboratory of Physico-Chemistry of Mineral Materials and Their Applications, National Center for Research in Materials Sciences CNRSM, Technopole Borj Cedria, P.O. Box 73, Soliman 8027, Tunisia

[2] Higher Institute of Environmental Sciences and Technologies, Carthage University, P.O. Box 1003, Hammam-Lif 2050, Tunisia

[3] Laboratory of Probability and Statistics, Mathematic Department, Faculty of Sciences Sfax, University of Sfax, Road of Soukra Km 4, P.O. Box 1171, Sfax 3000, Tunisia

[4] Departamento de Física de la Materia Condensada, Facultad de Ciencias, Universidad de Zaragoza, 50009 Zaragoza, Spain

[5] Instituto de Nanociencia y Materiales de Aragón (INMA), CSIC—Universidad de Zaragoza, Campus Río Ebro, 50018 Zaragoza, Spain

* Correspondence: jesus_spirit69@hotmail.com

Abstract: Many of the current strategies for removing pollutants from water are based on nanomaterials and nanotechnology. Lower values of Biological Oxygen Demand (BOD_5) and Chemical Oxygen Demand (COD) in water results in reduction in the amount of oxidizable pollutants. We present a study on the reduction of COD and BOD_5 in water from Wadi El Bey River (Tunisia), using magnetite nanoparticles (MNPs) and magnetic fields. The COD and BOD_5 removal reached values higher than 50% after 60 min, with optimum efficiency at pH values of ≈8 and for MNPs concentrations of 1 g/L. The use of a permanent magnetic field (0.33 T) showed an increase of COD and BOD_5 removal from 61% to 76% and from 63% to 78%, respectively. This enhancement is discussed in terms of the MNPs coagulation induced by the magnetic field and the adsorption of ionic species onto the MNPs surface due to Fe_3O_4 affinity.

Keywords: magnetite; Biological Oxygen Demand (BOD_5); Chemical Oxygen Demand (COD); magnetic field

1. Introduction

The availability of drinking water has become one of the most pressing environmental concerns nowadays. Human activities generate wastes that can affect the flowing water, modifying its chemical, physical, and biological properties, with high impact on its availability for human consumption. Water quality is a measure of whether water can affect human health and the balance of the ecosystem [1], and as such is a key part of any development of new technology to eliminate pollutants to contribute to the global water cycle. Synthetic drugs are large emerging class of pollutants, and their presence in water basins poses a serious threat to the environment. The accumulation of these pollutants is favored by their stability and resistance to biodegradation. Moreover, new drugs are required to have high water solubility to be efficient in clinics and this further increases their biological activity as pollutants [2].

Water quality assessment and sanitation infrastructure have not matched population growth and industrial development, especially in underdeveloped countries [3]. Rivers continue to be the main source of water for domestic, industrial and agricultural activities, and wastewater is often discharged directly into basins without any treatment, causing

severe degradation of water quality and the receiving environment. Therefore, awareness of the importance of surface water quality for public health and the environment has increased and many studies have been devoted to assessing surface water quality and preventing its impact on the environment [4].

Tunisia faces water scarcity with only about 450 m^3/inhabitant/year of available freshwater due to its arid to semi-arid climate [5]. There is an urgent need to protect water resources, address water scarcity and meet some of the increased demand. The Wadi El Bey watershed (475 km^2) is located in the north-eastern of Tunisia and flows through the Grombalia, Beni Khaled and Soliman plains [6]. It is located between Jebal Bouchoucha and Jebal Halloufa to the west, Jebal Abderrahman to the east, Jebal Reba El Ain to the south and the Gulf of Tunis to the north [7]. The Wadi El Bey River receives "pre-treated" water from different local industrial manufactures, however, still affecting negatively the physicochemical and microbiological quality of the river flow water.

For the water quality determination, the Biochemical Oxygen Demand (BOD$_5$) and the Chemical Oxygen Demand (COD) are the most common parameters to assess water quality, and their maximum concentration allowed depend on water use. The BOD$_5$ refers to the mass of Dissolved Oxygen (DO) consumed by living microorganisms as they break down organic matter in water, while the COD is the amount of oxygen consumed when water is chemically oxidized [8].

High levels of BOD$_5$ and COD cause a reduction in dissolved oxygen in the water and low concentrations cause eutrophication and harm aquatic life. It is therefore important to reduce the COD and BOD$_5$ parameters to levels that allow the safe discharge of wastewater into the river. COD values less than 30 mg/L and BOD$_5$ values less than 250 mg/L according with the ISO standard (International Organization for Standardization) requirements for the discharge of polluted water to the aquatic environment (environmental protection). In particular, COD and BOD$_5$ must be below 30 and 90 mg/L according to the Tunisian standard NT.106.002 (1989).

Current methods for removing pollutants from wastewater are still expensive and resource-intensive [9]. Recent attention has focused on the use of nanomaterials to reduce COD and BOD$_5$ levels as strategy for addressing ecosystem safety concerns. Nanotechnology based attempts have been made using magnetic nanoparticles (MNPs) for removal of organic pollutants and heavy metals from running water and wastewater [10].

The use of MNPs is highly desirable in many respects, some of the properties and responses to be mentioned, are: high specific surface interaction with molecules and ions (surface to volume ratio); high absorption efficiency [11]; lack of penetration resistance due to the elimination of internal absorption surfaces in porous adsorbents [12]; and the ability to be efficiently removed from water after treatment with magnets [13]. These properties of MNPs are strongly dependent on characteristics such as composition, size, morphology, magnetic properties as well as surface area and defects.

Iron oxides have much attention in water treatment strategies due to their magnetic properties. The use of magnetite (Fe$_3$O$_4$) has been explored as remediation agents in advanced oxidation processes [14], magnetized coagulation [15], or adsorption and removal of pollutants from water as recyclable heterogeneous catalyst [16]. MNPs composed of Fe$_3$O$_4$ as a catalyst support have been investigated due to their size and shape control and non-toxic properties [17].

Different synthesis methods have been developed to produce Fe$_3$O$_4$ MNPs with good control over particle properties. Combustion synthesis is a simple and inexpensive route to obtain MNPs that can be scaled up for environmental applications. It has been previously demonstrated [18] that combustion synthesis of Fe$_3$O$_4$ is influenced by the reaction atmosphere and the fuel used. Also, previous reports [19] showed that using the combustion method MNPs with extremely high surface area could be synthesized.

The use of MNPs in water remediation strategies exploit the magnetic coupling between an external magnetic field and the magnetic moments of the MNPs as a way to collect and recover the active materials from water. It enhances the process of impurity

removal by allowing the separation of targeted contaminants from the fluid stream [20]. The process usually involves embedding a magnetic substance within adsorbing materials or active molecules. By the use of a magnetic field gradient a magnetic force is produced on the MNPs and they can be separated from the fluid stream by an appropriate design of a magnetic field. It selectively targets specific contaminants, thus improving the efficacy of the adsorption process, which leads to higher removal rates and more effective treatment of polluted water [21].

The effects of the application of a magnetic field on the efficiency for reduction of organics in wastewater using magnetite nanoparticles have been previously investigated [22]. The application of the magnetic field favors the disturbance of the laminar flow, thus generating useful mixing patterns to promote the intimate interaction of the nanoparticles with other components present in the solution. A previous study [23] on the activity of magnetite NPs under a DC magnetic field of 20 mT demonstrated the possibility of improving degradation after 48 h of application.

This work presents results on the efficiency of the MNPs for the removal of COD and BOD_5 in polluted water from the Wadi El Bey river (Tunisia). The removal efficiency was increased by 15% by combining Fe_3O_4 nanoparticles with a magnetic field. The magnetic field enhances the removal of COD and BOD_5 and assists in the separation of the MNPs.

The Wadi El Bey watershed, located in the northeastern of Tunisia between $36°35'00''$–$36°42'00''$ N and $10°28'00''$–$10°33'00''$ E, covers an area of 475 km^2 and drains the Grombalia plain. The region has potential evapotranspiration of about 1300 mm/year, and is higher in summer due to increased temperature and decreased air hymidity. Industrial effluents (textile, tannery, food industry, etc.), agricultural drainage, untreated urban and tourist wastewater, etc. have contributed to the pollution of the Wadi El Bey River [24]. It has been reported that Wadi El Bey Soliman display COD values up to 677 mg/L and BOD_5 up to 326 mg/L, with turbidity levels of up to 1080 NTU (with pH values 6.6 to 8.5) [25]. Nitrate levels are well above the 50 mg/L limit of set by Tunisian standards, reaching worrying levels of up to 159 mg/L [26,27]. At all river sites, COD values exceeded the permissible limit of 90 mg O_2/L according to Tunisian standards (TN-106-002). This confirms the relevance of the pollution problem from industrial and agricultural discharges.

2. Materials and Methods

2.1. Synthesis of MNPS

The reagents used for combustion synthesis of the magnetic material were: Ferric nitrate nonahydrate (Fe $(NO_3)_3 9H_2O$, $\geq$99.95%) as raw reactant and glycine ($C_2H_5NO_2$) as fuel (Merck KGaA, Darmstadt, Germany). A schematic representation of the employed methodology is presented in Figure 1.
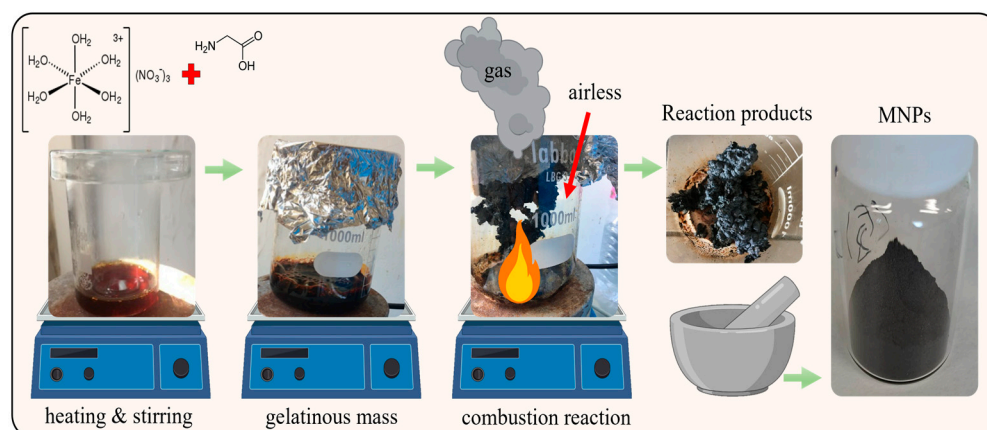

Figure 1. Steps of the performed combustion method. After mixing the raw reactant and the fuel, the combustion reaction products were grinded until reaching fine powder composed by magnetic nanoparticles (MNPs).

First, $Fe(NO_3)_3$ and $C_2H_5NO_2$ were dissolved in 150 mL of deionized water under stirring to prepare homogeneous solution. The solution was then poured into a 1000 mL beaker and heated contentiously on a temperature-controlled hotplate until it evaporated and developed into a viscous gelatinous mass. After a few minutes, a violent self-propagating and non-explosive combustion reaction suddenly took place, leading to the formation of MNPs, accompanied by the liberation of voluminous gases. The result of the combustion reaction was collected and ground in a mortar to a fine powder. This powder was stored at room temperature for further characterization.

2.2. Characterization Techniques

The physical and chemical properties from of the obtained MNPs were characterized using different techniques. Morphology and particle size were determined using Transmission Electron Microscopy (TEM) image analysis using a FEG TECNAI T20 at 200 kV and Image J software (1.56t version). Diluted dispersions containing MNPs were prepared and a 10 μL drop was placed on Holley-carbon copper grids for observation and imaging. The crystal structure of the as prepared product was examined using a Bruker D8 Advance high-resolution X-ray powder diffractometer (XRD) using Cu Kα radiation (λ = 1.5418 Å) in Bragg-Brentano configuration. For compositional analysis, Perkin Elmer Frontier Fourier Transform Infrared (FTIR) spectrometer for the identification of molecular vibrations in the samples, and energy dispersive spectroscopy (EDS) was developed using a Quanta FEG 650 Scanning Electron Microscope (SEM) equipped with ThermoFisher® X-Ray photon detector. Surface area and porous size measurements were performed using 120 mg of as prepared MNPs in a TriStar 3000 (Micromeritics, Norcross, GA, USA) analyzer and the calculations were obtained using the TriStar 3000 V6.08 A version software.

2.3. COD and BOD_5 Measurements

Previously collected samples from the river effluent were filtered to avoid turbidity affecting the test results. Standard methods for testing polluted water were used to measure COD and BOD_5 values according to the protocol referenced in the Standard Water and Wastewater Testing Methods (COD and 5210-B Part 5220-B) [28] at 174 and 340 mg/L, respectively.

For the COD measurements, the water samples (2 mL) were placed in a culture tube and 1 mL of $K_2Cr_2O_7$ was added to the solution. The sulfuric acid reagent solution (3 mL) was then carefully poured into the container to form an acid layer under the sample digestion layer. The tube containing the mixture was placed in a block cooker preheated to 150 °C and refluxed for 2 h. Then, after cooling the sample to room temperature, 2 drops of ferritin indicator are added to the solution under stirring and titrated with standard 0.10 M FAS. At the end, the color change from blue-green to reddish-brown.

BOD_5 was measured by the respiration method, which allows the direct measurement of the oxygen consumption of microorganisms from air or an oxygen-enriched environment in a closed vessel under constant conditions. Respirometry measures oxygen consumption continuously over time. The oxygen tank is the column of air above the sample. As with standard methods, dilution is required. Vials are hermetically sealed to prevent interference from external atmospheric pressure. Oxygen is provided by constant stirring (a magnetic stir bar helps diffuse oxygen into the sample). Carbon dioxide is formed when heterotrophic bacteria oxidize organic matter.

As CO_2 is produced, it is removed from the system by absorbing sodium hydroxide and the pressure change is recorded. The change in pressure is directly proportional to the CO_2 produced. i.e., O_2 consumed, the final value was converted to an equivalent BOD_5 value. The amount and removal efficiency (%) of COD and BOD_5 (mg/g) on MNPs at each time point were calculated by the following Equation (1) [29].

$$R\% = \frac{C_0 - C_f}{C_0} \qquad (1)$$

where C_0 and C_f are the initial and final concentrations of COD and BOD$_5$ (mg/L).

The COD and BOD$_5$ assessments were evaluated in function of different experimental parameters: contact time; concentration of MNPs, pH and stirring rate speed.

3. Results

The MNPs were synthetized by combustion methods using Fe(NO$_3$)$_3$ as precursor and C$_2$H$_5$NO$_2$ as combustible.

3.1. MNPs Size and Structure

The bright field TEM image of the obtained MNPs presented in Figure 2a show the typical agglomerated state expected when it comes to magnetic nanostructures. Large clusters were founded during the sample's observation, but results evident that those clusters are composed by small particles. As inset in Figure 2a, the histogram from particle size distribution analysis (n = 200 particles) shown that most of the particles in the sample fall within a certain size range around the average ($\phi = 17 \pm 6$ nm), but there may also be some particles that are larger or smaller.
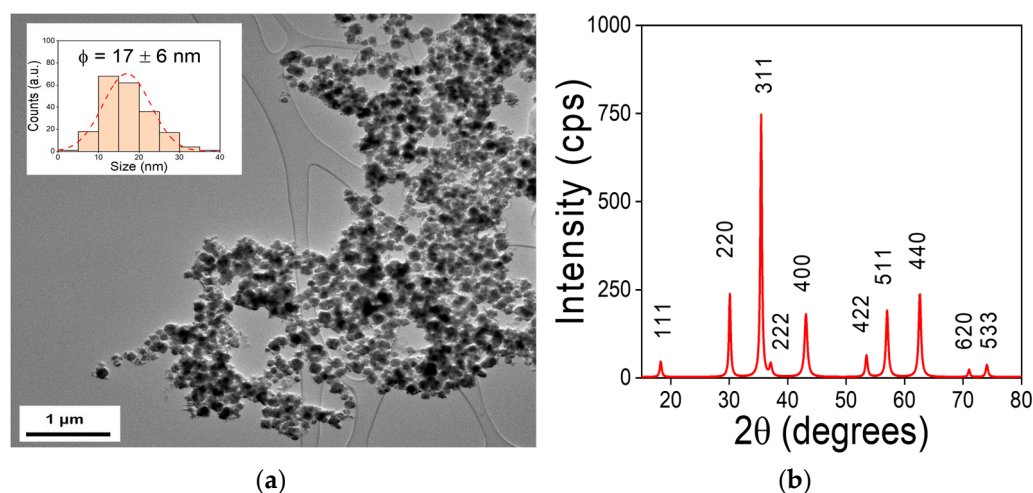

(**a**)	(**b**)

Figure 2. Particle size and structure of MNPs produced by the combustion method: (**a**) bright field TEM micrograph of MNPs samples, and as inset size distribution histogram revealing average diameter $\phi = 17 \pm 6$ nm; (**b**) X-ray diffractogram from powder samples of as-obtained MNPs identifying the different crystalline planes reflections associated to the magnetite structure (JCPDS 19-629).

The XRD patterns from obtained MNPs presented in Figure 2b is associated to magnetite (Fe$_3$O$_4$) compound. All diffraction peaks of the X-ray diffractogram are indexed according to JCPDS 19-629 of magnetite-type iron oxide. The elaborated MNPs belong to the space group Fd-3m whose mesh parameter is a = 8.3940 Å [30]. The peak width and absence of unexplained peaks confirmed the crystallization and high purity of the nanoparticle-sized magnetite. The average crystal size of magnetite nanoparticles was estimated using Equation (2) [31]

$$D = \frac{K * \lambda}{\beta * cos\theta} \tag{2}$$

where D is the average crystal size, λ is the X-ray radiation's wavelength (1.5406 Å), K is the dimensionless form factor (0.9, in this case), β is the line's FWHM (full width at half maximum) in radians, and θ is the Bragg's angle in degrees [32]. The FWHM of the major peak ($2\theta = 35.405°$) of XRD patterns, the nanomaterials that were synthesized had an average crystalline size of about 17.6 nm. Comparison with the literature [33,34] reveals that the average crystalline size analyzed the X-ray diffraction (XRD) patterns of magnetite nanoparticles obtained at different temperatures. The observed diffraction peaks

corresponded to the crystal planes of Fe_3O_4 thus confirming the purity of the obtained particles. Furthermore, it was observed that and increasing the annealing temperature lead to a decrease in the width at half height of the reflection peaks, consistent with the expected crystallite size and an improvement in their sharpness. This suggests an increase in the size of the Fe_3O_4 nanoparticles and an improvement in there and crystallinity.

The Scherrer formula was used to calculate the particle size from the broadening of the X-ray diffraction peaks. The results show that the size of Fe_3O_4 nanoparticles increases in the annealing temperature range of 200–400 °C. The average sizes of the particles synthesized at different temperatures were determined and indicate a progressive increase in size with increasing temperature.

These results are consistent with other previous studies and highlight the importance of annealing temperature in the synthesis and properties of magnetite nanoparticles. Understanding these growth mechanisms is essential to explore the potential applications of these nanoparticles in various fields of research and applications.

3.2. MNPs Composition

Examination of the FTIR spectrum shows a strong absorption band at 560 cm^{-1} associated with the stretching vibration of Fe–O functional groups typical of the crystalline lattice of magnetite (Fe_3O_4) [35–37]. The intense band at 1380 cm^{-1} and centered at 1100 cm^{-1} are due to residual NH_4^+ in prepared simple. The vibration detected at 1040 cm^{-1} is associated with the CO-O-CO tension in carbon dioxide released during combustion. Other material vibration modes are appeared at 3500 cm^{-1} and 1750 cm^{-1} are attributed to hydrogen-bonded water molecules vibrations adsorbed on the surface and O-H bending vibration [38,39]. Our result is in agreement with the results of other works, which affirmed that the presence of magnetite can be seen by wide strong absorption band between 540 and 630 cm^{-1} [40], especially for Fe–O bond of bulk magnetite at 576 cm^{-1}. Referring to the work of [41] magnetite can be presented in the form of crystals with continuous bonds and the atoms are bound together with equal forces (ionic, covalent or van der vales force). According to these results, the vibration modes appeared at around 440 cm^{-1} and 560 cm^{-1} are related to Fe–O bonds and are respectively attributed to octahedral and tetrahedral sites [42].

The secondary electron SEM micrograph presented in Figure 3b reveal the large clusters formed by the agglomeration on MNPs in powder. Some authors suggested that the agglomeration of nanoparticles was caused by the Van Der Waals forces due to operating conditions and drying [43]. Also, the presence of residual water enhances the agglomeration of nanoparticles with nanometric size in the order of several micrometers. The obtained EDS spectrum confirms the presence of elements Fe (73.24%), O (20.39%) and C (6.37%) in the sample.

3.3. MNPs Surface Area Analysis

Brunauer-Emmett-Teller (BET) analysis is a widely used method to determine the specific surface area of a material. This method involves the measurement of gas adsorption on the surface of a solid material at different pressures, allowing the determination of the surface area by analyzing the adsorption isotherm. The obtained surface area is critical in determining the ability of the material to adsorb different molecules from contaminated water or gases. BET analysis also provides information on the porosity of the material, such as pore volume and pore size distribution, which can influence its adsorption capacity [44].

The powder specific surface area and porosity distribution of MNPs were analyzed using the BET technique. These parameters are critical in determining the ability to adsorb and remove various molecules from contaminated water. The obtained BET surface area of 16.82 ± 0.01 m^2/g. While the pore volume about 0.04 cm^3/g and the pore size 10.66 nm.
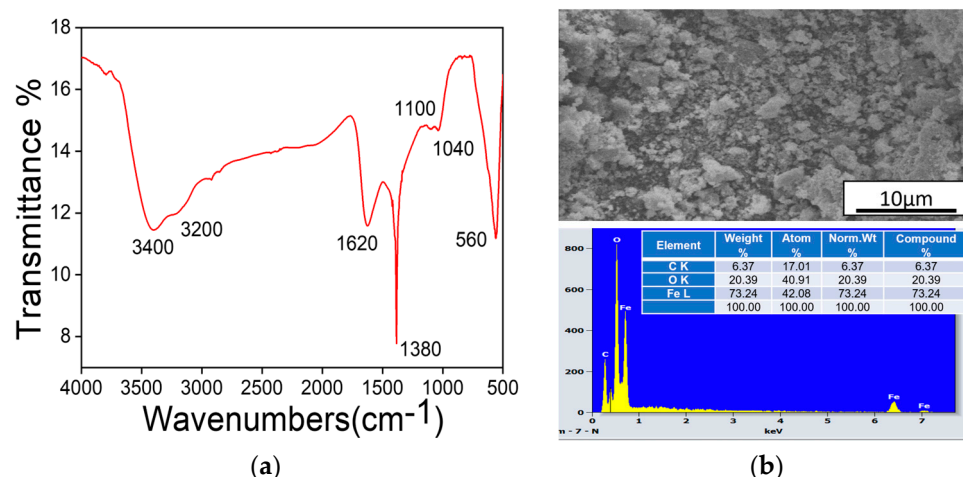
Figure 3. MNPs composition: (**a**) vibrational normal modes from MNPs functional groups detected in FTIR−ATR; (**b**) secondary electrons SEM image showing agglomerated clusters and EDS spectrum at 10 kV from MNPs samples in powder.

According to the isotherm shown in Figure 4, the obtained MNP behaves like a type II isotherm, this type of isotherm indicates an indefinite multi-layer formation after completion of the monolayer and is found in adsorbents with a wide distribution of pore sizes (inset). Upon completion of a monolayer, successive layer adsorption occurs, forming the observed inflection point. This behavior is characteristic of adsorbents that they are capable to adsorb more efficiently the gas molecules, for instance water vapor on activated carbon [45]. However, the large surface area of MNPs is suitable for adsorption and heterogeneous surfaces for be reached using this kind of materials. Moreover, functional groups present on the MNPs surfaces can improve the interactions with ions, molecules and large particles present in the wastewater from the Wadi El Bey watershed.
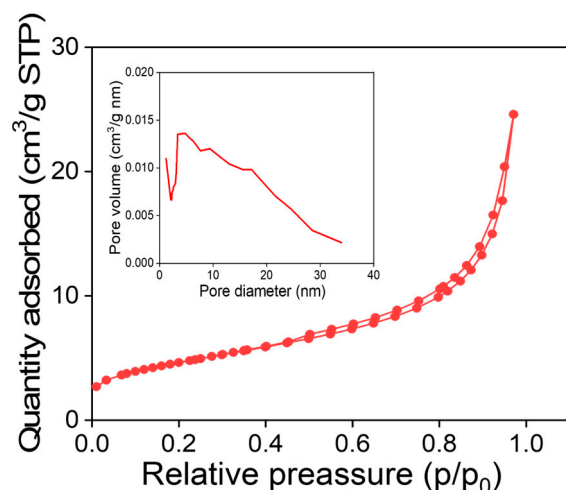

Figure 4. N_2 adsorption isotherm from MNPs elaborated using combustion method, as inset broad pore diameter distribution can be observed.

3.4. Removal Efficiency Using MNPs within the BOD_5 and COD Experiements

The obtained MNPs were evaluated as water's quality enhancers in a series of experiments to observe the effect of the different experimental conditions on its performance reducing BOD_5 and COD. The Figure 5 summarizes the results from the experiments using MNPs under different contact time (Figure 5a), concentration (Figure 5b), pH (Figure 5c), and stirring velocity (Figure 5d).
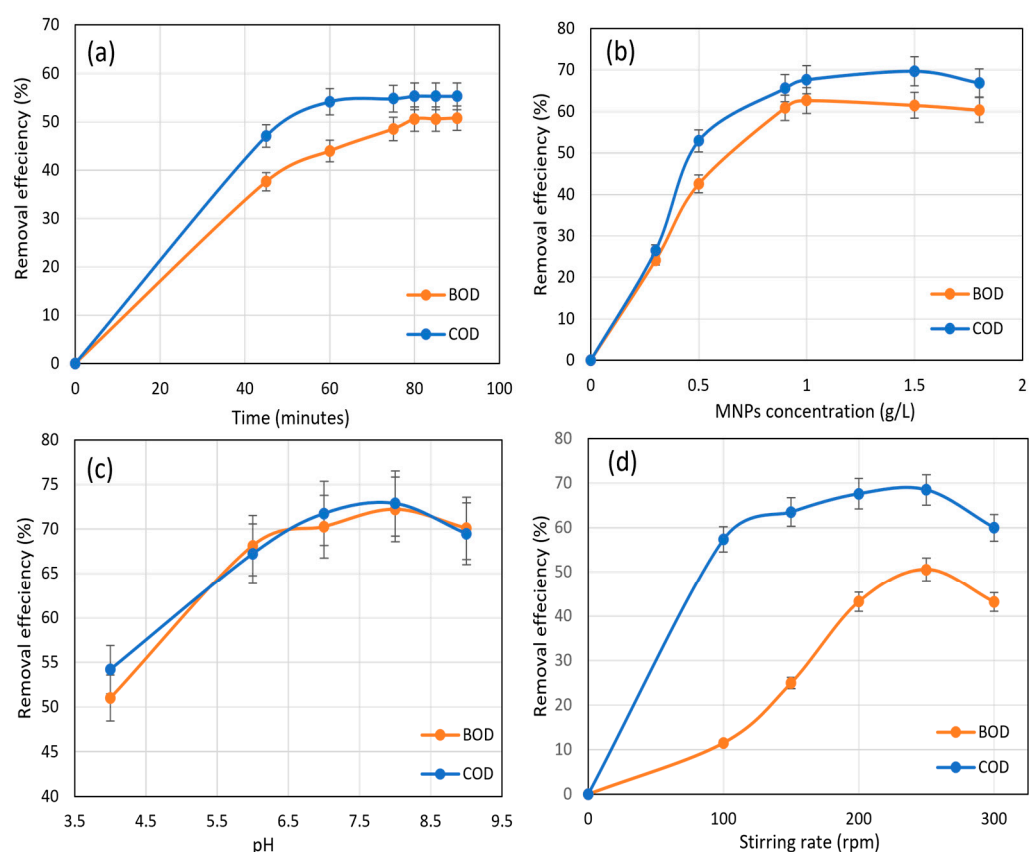
Figure 5. COD and BOD$_5$ removal efficiency using MNPs at different experimental conditions: (**a**) the effect of the contact time using 1 g/L of MNPs at 45–90 min interval; (**b**) the effect of MNPs using 0.3–1.8 g/L concentrations, pH = 8; (**c**) the effect of the pH conditions, evaluating from 4 to 9 values (1 g/L of MNPs, 200 rpm); and (**d**) the stirring rate effect evaluated from 100 to 300 rpm during 80 min.

The optimum contact time was evaluated in the experiments using 1 g/L MNP. The pH of the contaminated water was kept at 8 and the stirring speed was approximately 200 rpm at a room temperature of 20 ± 1 °C. Times of 45, 60, 75, 80, 85 and 90 min, respectively were evaluated during the experiments. The obtained results showed that the high values of COD and BOD$_5$ removal efficiencies reached 55% and 50% within 80 min at the lowest limit. However, the results showed that the COD and BOD$_5$ removal efficiencies stabilized after a contact time of 80 min. Regarding the magnetic performance of the Fe$_3$O$_4$ nanoparticles produced by the present combustion route, it is clear from the magnetic moment of the nanoparticles was enough to produce the magnetic separation observed during experimental runs.

Using 80 min as optimal parameter, the COD and BOD$_5$ were evaluated using different concentrations of MNPs, ranging 0.3–1.8 g/L. The removal efficiency was increased as the MNPs concentration increased as can be observed in Figure 5b, but some differences were founded between COD and BOD$_5$. For COD, the removal efficiency reaches their maximum (70%) at 1.5 g/L MNPs doses, whereas for BOD$_5$, the optimal value of MNPs concentration was founded at 1 g/L for removal efficiency of 63%.

The influence of the pH on the reduction of oxidizable components in wastewater using MNPs were explored emulating acidic, neutral, and alkaline conditions (pH 4, 6, 7, 8, and 9) for COD and BOD$_5$ concentrations (340 and 174 mg/L, respectively), using 1 g/L of MNPs and contact period 80 min as optimal parameters with stirring rate 200 rpm at ambient temperature 25 ± 1 °C. The removal efficiency for COD and BOD$_5$ were 54, 67, 71, 73, 70% and 51, 68, 70, 72, and 70%. Therefore, a value of pH = 8 was selected as the optimal condition for removal efficiency.

Stirring speed was also a factor studied for removal efficiency of COD and BOD_5, since the unavoidable agglomeration of the MNPs in aqueous solutions could influence the results. We evaluated stirring speeds ranging from 100 to 300 rpm. The removal efficiencies in function of the agitation speed for COD and BOD_5 can be observed in Figure 4d. Removal efficiency of 57, 63, 67, 68, and 60% for COD and 12, 25, 43, 50 and 43% for BOD_5 were obtained, choosing 250 rpm as the best agitation value.

Using the previously set of parameters as the most efficient for removal of COD and BOD_5 in polluted water, we aimed to minimize the variability in the results from MNPs coagulation y applying an external dc magnetic field of H = 0.33 T keeping the contact time of 80 min, pH of 8, MNPs concentration of 1.5 g/L, and a stirring speed of 250 rpm. The results in Figure 6 show a clear COD removal increasing from 61% to 76%, and from 63% to 77% on BOD_5 measurements.
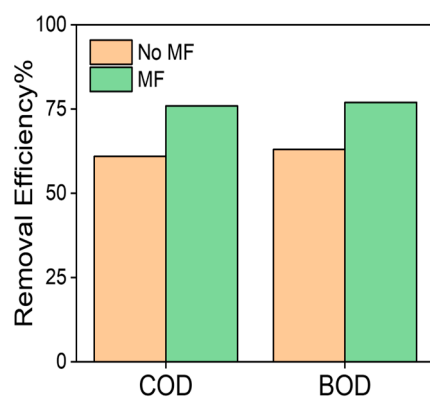

Figure 6. Improvement on removal efficiency of oxidizable pollutants in waste water using magnetic nanoparticles and magnetic separation (0.33 T).

3.5. Regeneration Efficiency

To evaluate the reusability of the Fe_3O_4 magnetic nanoparticles in the presence of a magnetic field for COD, BOD_5 removal from polluted water, five successive regeneration cycles were carried out, and the COD, BOD_5 removal of regeneration Fe_3O_4 magnetic nanoparticles applying an external magnetic field of H = 0.33 T. Each treatment cycle experiment was run keeping the contact time of 80 min, pH of 8, MNPs concentration of 1.5 g/L, and a stirring speed of 250 rpm.

In three regeneration cycles of Fe_3O_4 magnetic nanoparticles experiments for COD, BOD_5 removal, the reduction percentages of DCO and BOD_5 were found to be 76% and 77%, respectively. After the first regeneration, the reduction percentages decreased slightly to 69% for COD and 70% for BOD_5. The reduction percentages decreased further after the second regeneration to 61% for COD and 63% forBOD_5. After the third regeneration, the reduction percentages decreased further to 56% for COD and 58% for BOD_5.

Overall, these results observed in Figure 7 suggest that the magnetic nanoparticles used in this study have good potential for the treatment of polluted water. However, as the number of regenerations increases, the efficiency of the nanoparticles decreases, which may limit their practical application value. In order to determine the regeneration of magnetic nanoparticles for the treatment of polluted water, several conditions must be taken into account, such as the type of pollutants, the concentration of nanoparticles used, the contact time, the pH, the temperature and the number of regeneration cycles and the regeneration method used.
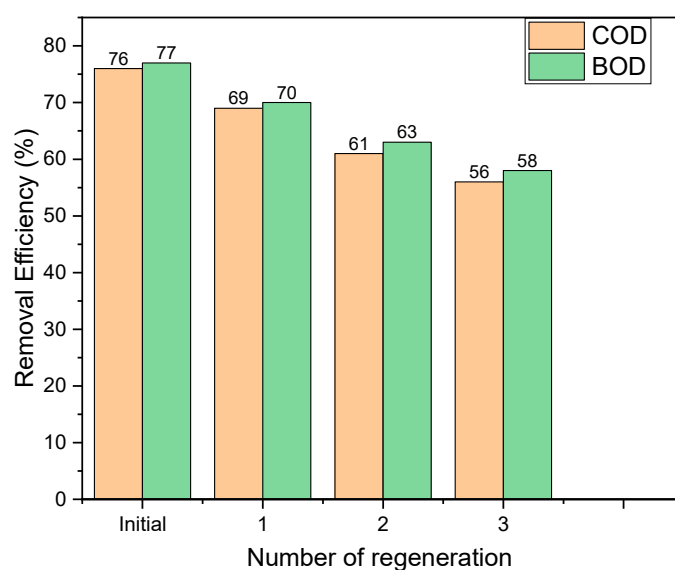
Figure 7. Evaluation of the removal efficiency of nanoparticles during regeneration cycles.

4. Discussion

The characterization results positioning to the combustion method employed for the synthesis as feasible method to produce on a facile way MNPs with adequate properties such as size, crystallinity, surficial area and functional groups for their application as removal agents in the oxidizable pollutant removal applications.

In the evaluation of MNPs as enhancers of the quality of water, some findings can be summarized as follows. The contact time must be at least 80 min to achieve maximum efficiency. In a previous work by Ahmed S. Mahmoud et al. [46], the effect of contact time on COD and BOD_5 removal efficiency using green synthesis nano-iron extracted from black tea has been studied. They found that the optimal time was 60 min with a removal efficiency of 87.9 and 100% for COD and BOD_5 respectively. Moreover, Rasha A. Sary El-deen et al. [47] worked on the removal of COD from Domestic Wastewater using Entrapped Sewage Sludge Ash and the effective time was 60 min with a removal efficiency of 78% for an initial COD concentration 400 mg/L.

In the work of Rabie S. Farag et al. [48] who studied the removal of chemical oxygen demand from aqueous solution using the expensive nano zero valent iron (nZVI) compared to Fe_3O_4, the optimum removal time was 20 min for COD removal. Also, Nashaat N. Nassar et al. [49] worked on the treatment of olive mill based wastewater by means of magnetic nanoparticles the effective time for COD removal was 30 min. In general, literature findings showed that the optimal time for COD and BOD_5 removal using magnetite NPs is between 20 and 120 min and our result is similar with most works.

Soliman et al. [50] and Umoren et al. [51] have proven that the increasing of adsorbent quantity will increase the number of active sites, adsorbent surface and availability of molecules to adsorbent surface. So, the probability of contact and adsorption will increase while increasing the mass of nanoparticles. However, by increasing the amount of adsorbent, the risk of formation of solid aggregate and the decrease in apparent porosity and also the decrease in nanoparticle mobility will cause a difficulty in the diffusion of molecules in the adsorbent and will then decrease the efficiency of adsorption.

We can then conclude that the optimal mass of magnetite nanoparticles is 1.5 g/L. The difference in absorptionBOD$_5$ and COD is due to differences in the carbon chain, the solubility of ingredients them and surface tension to the absorbent surface. The similar results were reported in elimination of aniline and surfactant and total organic carbon with Fe_3O_4 nanoparticles and activated carbon-Fe_3O_4.

The results show that the removal efficiency was the highest at pH = 8 under slightly alkaline conditions. This result can be attributed to the strongly acidic medium, where

small magnetite particles are decomposed under the influence of acid, leaving NPs in vacancies and affecting the adsorption activity. On the other hand, the excess OH- ions in the strong alkaline solution can enhance the removal rate of COD and BOD_5 by activating the adsorption sites with negatively charged ions. In this case, similar results were obtained by Sahu et al. [52] using different adsorbent materials for sewage removal, showing an effective pH = 8.

Stirring speed of 250 rpm seemed enough to allow maximum adsorption conditions (i.e., avoiding coagulation while adsorption onto the MNPs takes place), with no further removal effectiveness at higher stirring speeds. Previous investigations reported the removal of COD from aqueous solutions using conventional methods, such as SSA adsorption and aluminum sulfate coagulation that took place between 300 and 500 rpm, consistent with these results [53].

Magnetite nanoparticles of Fe_3O_4 are known to act as efficient adsorbents [54], due to the hydroxyl groups on the surface of Fe_3O_4, that can generate positive or negative charges through protonation or deprotonation by pH changes in aqueous solution, making this material a good option to adsorb and remove ionic species from water through electrostatic interactions [55]. The positively-charged Fe ions in Fe_3O_4 also serve as adsorption sites for negatively charged species or electron-rich functional groups of certain organic pollutants. Furthermore, the surface of Fe_3O_4 can be modified to improve functionalization and protect the core from demagnetization [56].

The present results reveal that the adsorption performance of Fe_3O_4 can be enhanced by magnetic coupling to remove COD and BOD_5. Based on the work of Brown and Barnwell [57] a strong correlation was found between different types of microorganisms and the horizontal magnetic field vector. This study also supports Tomska and Wolny's observation of increased degradation of organic matter [58]. They showed that nitrogen compounds respond positively to an MF (magnetic field) with an induction strength of 40 mT. The good adsorption efficiency and high recoverability of the Fe_3O_4 MNPs using magnetic fields, with the low cost and potential scalability of their production to match industrial requirements, make this approach competitive as a future strategy against the hurdles of large basin-s wastewater decontamination.

In summary, this study reveals a new finding that the presence of a magnetic field can enhance the adsorption of organic pollutants onto magnetite nanoparticles, resulting in increased efficacy in the reducing of COD and BOD_5. The underlying mechanism behind this phenomenon is the physical forces, namely Van der Waals interactions, which alter the molecular structure, surface charge, and interactions between the organic molecules and nanoparticles. This mechanism is likely to be affected by the applied magnetic field by improving the diffusion of molecules, resulting in more efficient adsorption and greater reduction in COD and BOD_5. The present method overcomes enhances the separation and recovery of the nanoparticles, ultimately improving the overall efficiency and efficacy of the treatment process. However, this study does not claim to be complete and further research is needed. For instance, the effect of magnetic field on adsorption, the optimal magnetic field strength, the selectivity of adsorption, and the operating conditions of the treatment need to be further investigated.

In conclusion, this study has demonstrated, for the first time, that the presence of a magnetic field enhances the adsorption of organic pollutants on magnetite nanoparticles. The enhanced removal of COD and BOD_5 is attributed to the influence of magnetic field on the molecular structure, surface charge, and intermolecular interactions between the nanoparticles and organic molecules, mediated by physical forces such as Vanderwaals interactions. Thus, magnetic field application is a promising approach that can improve wastewater treatment and facilitate the separation and reuse of magnetite nanoparticles. However, further research is needed to fully explore the effects of the magnetic field on adsorption, including the optimal field intensity, selectivity of adsorption, and treatment operating conditions. Magnetite nanoparticles synthesized by combustion method revealed an excellent adsorbent for the removal of organic matter in polluted water. After a contact

time of 80 min, pH 8, magnetite NPs 1.5 g/L, and a stirring speed of 250 rpm, the best reduction efficiencies of COD and BOD_5 were 61% and 67%, respectively. The studied Fe_3O_4 NPs were found to be more effective in removing COD and BOD_5 by using a coupling process magnetic with a strength of 0.33 T, which improves the removal efficiency by 15% from 61 to 76 for COD and by 14% from 63 to 78 for BOD_5.

Author Contributions: Conceptualization, J.A.F.-G., H.T., A.E. and M.F.; methodology, J.A.F.-G., H.T., A.E., N.A., M.F. and G.F.G.; software, J.A.F.-G., A.E. and N.A.; validation, M.F., K.H.-N., G.F.G. and J.A.F.-G.; formal analysis H.T., G.F.G. and J.A.F.-G.; investigation, K.H.-N. and N.A.; resources, H.T. and N.A.; data curation, J.A.F.-G., H.T. and G.F.G.; writing—original draft preparation, H.T. and J.A.F.-G.; writing—review and editing, G.F.G. and M.F.; supervision, K.H.-N., A.E. and M.F.; funding acquisition, G.F.G. and K.H.-N. All authors have read and agreed to the published version of the manuscript.

Institutional Review Board Statement: Not applicable.

Informed Consent Statement: Not applicable.

Data Availability Statement: The data presented in this study are available on request from the corresponding author.

Conflicts of Interest: The authors declare no conflict of interest.

References

1. Wang, Y.; Wang, P.; Bai, Y.; Tian, Z.; Li, J.; Shao, X.; Mustavich, L.F.; Li, B.L. Assessment of Surface Water Quality via Multivariate Statistical Techniques: A Case Study of the Songhua River Harbin Region, China. *J. Hydro-Environment Res.* **2013**, *7*, 30–40. [CrossRef]
2. Sayadi, M.H.; Chamanpour, E.; Fahoul, N. The Ultrasonic Process with Titanium Magnetic Oxide Nanoparticles to Enhance the Amoxicillin Removal Efficiency. *J. Water Environ. Nanotechnol.* **2022**, *7*, 241–251. [CrossRef]
3. Ahmed, W.; Vieritz, A.; Goonetilleke, A.; Gardner, T. Health Risk from the Use of Roof-Harvested Rainwater in Southeast Queensland, Australia, as Potable or Nonpotable Water, Determined Using Quantitative Microbial Risk Assessment. *Appl. Environ. Microbiol.* **2010**, *76*, 7382–7391. [CrossRef]
4. Davies, J.M.; Mazumder, A. Health and Environmental Policy Issues in Canada: The Role of Watershed Management in Sustaining Clean Drinking Water Quality at Surface Sources. *J. Environ. Manag.* **2003**, *68*, 273–286. [CrossRef] [PubMed]
5. Louati, M.E.H.; Khanfir, R.; Alouini, A.; El Echi, M.L.; Frigui, L.; Marzouk, A. Guide Pratique de Gestion de La Sécheresse En Tunisie. Available online: http://www.citet.nat.tn/Portail/doc/SYRACUSE/20391/guide-pratique-de-gestion-de-la-secheresse-en-tunisie (accessed on 31 March 2023).
6. Khadhar, S.; Mlayah, A.; Chekirben, A.; Charef, A.; Methammam, M.; Nouha, S.; Khemais, Z. Vecteur de La Pollution Metallique Du Bassin Versant de l'Oued El Bey Vers Le Golfe de Tunis (Tunisie). *Hydrol. Sci. J.* **2013**, *58*, 1803–1812. [CrossRef]
7. Gasmi, T.; Khouni, I.; Ghrabi, A. Assessment of Heavy Metals Pollution Using Multivariate Statistical Analysis Methods in Wadi El Bey (Tunisia). *Desalination Water Treat.* **2016**, *57*, 22152–22165. [CrossRef]
8. Dębska, K.; Rutkowska, B.; Szulc, W.; Gozdowski, D. Changes in Selected Water Quality Parameters in the Utrata River as a Function of Catchment Area Land Use. *Water* **2021**, *13*, 2989. [CrossRef]
9. Wu, H.; Zhang, J.; Ngo, H.H.; Guo, W.; Hu, Z.; Liang, S.; Liu, H. A Review on the Sustainability of Constructed Wetlands for Wastewater Treatment: Design and Operation. *Bioresour. Technol.* **2014**, *175*, 594–601. [CrossRef]
10. Shukla, S.; Khan, R.; Daverey, A. Synthesis and Characterization of Magnetic Nanoparticles, and Their Applications in Wastewater Treatment: A Review. *Environ. Technol. Innov.* **2021**, *24*, 101924. [CrossRef]
11. Fortes, C.C.S.; Daniel-da-Silva, A.L.; Xavier, A.M.R.B.; Tavares, A.P.M. Optimization of Enzyme Immobilization on Functionalized Magnetic Nanoparticles for Laccase Biocatalytic Reactions. *Chem. Eng. Process. Process Intensif.* **2017**, *117*, 1–8. [CrossRef]
12. Mohsenibandpei, A.; Ghaderpoori, M.; Hassani, G.; Bahrami, H.; Bahmani, Z.; Alinejad, A.A. Water Solution Polishing of Nitrate Using Potassium Permanganate Modified Zeolite: Parametric Experiments, Kinetics and Equilibrium Analysis. *Glob. Nest J.* **2016**, *18*, 546–558. [CrossRef]

13. Liu, J.F.; Zhao, Z.S.; Jiang, G.B. Coating Fe_3O_4 Magnetic Nanoparticles with Humic Acid for High Efficient Removal of Heavy Metals in Water. *Environ. Sci. Technol.* **2008**, *42*, 6949–6954. [CrossRef] [PubMed]

14. Marcinowski, P.; Bury, D.; Krupa, M.; Ścieżyńska, D.; Prabhu, P.; Bogacki, J. Magnetite and Hematite in Advanced Oxidation Processes Application for Cosmetic Wastewater Treatment. *Processes* **2020**, *8*, 1343. [CrossRef]

15. Sibiya, N.P.; Rathilal, S.; Tetteh, E.K.; Amo-Duodu, G. Evaluation of The Effect Of Recycled Magnetized Coagulants On Wastewater Treatment. *J. Pharm. Negat. Results* **2022**, *13*, 3466–3472. [CrossRef]

16. Lourens, A.; Falch, A.; Malgas-Enus, R. Magnetite Immobilized Metal Nanoparticles in the Treatment and Removal of Pollutants from Wastewater: A Review. *J. Mater. Sci.* **2023**, *58*, 2951–2970. [CrossRef]

17. Masudi, A.; Harimisa, G.E.; Ghafar, N.A.; Jusoh, N.W.C. Magnetite-Based Catalysts for Wastewater Treatment. *Environ. Sci. Pollut. Res.* **2020**, *27*, 4664–4682. [CrossRef]

18. Ianoş, R.; Lazău, I.; Păcurariu, C. The Influence of Combustion Synthesis Conditions on the α-Al2O3 Powder Preparation. *J. Mater. Sci.* **2009**, *44*, 1016–1023. [CrossRef]

19. Mukasyan, A.S.; Dinka, P. Novel Approaches to Solution-Combustion Synthesis of Nanomaterials. *Int. J. Self-Propagating High-Temp. Synth.* **2007**, *16*, 23–35. [CrossRef]

20. Elaoud, A.; Turki, N.; Amor, H.B.; Jalel, R.; Salah, N.B. Influence of the Magnetic Device on Water Quality and Production of Melon. *Int. J. Curr. Eng. Technol.* **2016**, *6*, 2256–2260. [CrossRef]

21. Amor, H.B.; Elaoud, A. Characteristic Study of Some Parameters of Soil Irrigated by Magnetized Waters. *Arab. J. Geosci.* **2020**, *13*, 1007. [CrossRef]

22. Aragaw, T.A.; Bogale, F.M.; Aragaw, B.A. Iron-Based Nanoparticles in Wastewater Treatment: A Review on Synthesis Methods, Applications, and Removal Mechanisms. *J. Saudi Chem. Soc.* **2021**, *25*, 101280. [CrossRef]

23. Zieliński, M.; Dębowski, M.; Krzemieniewski, M. Effect of Constant Magnetic Field (CMF) with Various Values of Magnetic Induction on Effectiveness of Dairy Wastewater Treatment under Anaerobic Conditions. *Pol. J. Environ.* **2014**, *23*, 255–261.

24. Taoufik, G.; Khouni, I.; Ghrabi, A. Assessment of Physico-Chemical and Microbiological Surface Water Quality Using Multivariate Statistical Techniques: A Case Study of the Wadi El-Bey River, Tunisia. *Arab. J. Geosci.* **2017**, *10*, 181. [CrossRef]

25. Mhamdi, F.; Khouni, I.; Ghrabi, A. Diagnosis and Characteristics of Water Quality along the Wadi El Bey River (Tunisia). Coagulation/Flocculation Essays of Textile Effluents Discharged into the Wadi. *Desalin. Water Treat.* **2016**, *57*, 22166–22188. [CrossRef]

26. Akrout, H.; Baccouche, H.; Mellah, T.; Jomaa, S. Surface Water Quality Assessment of Wadi El Bey, Tunisia. In Proceedings of the 3rd Euro-Mediterranean Conference for Environmental Interration, Sousse, Tunisia, 10–13 June 2021; pp. 1–5.

27. Khouni, I.; Louhichi, G.; Ghrabi, A. Use of GIS Based Inverse Distance Weighted Interpolation to Assess Surface Water Quality: Case of Wadi El Bey, Tunisia. *Environ. Technol. Innov.* **2021**, *24*, 101892. [CrossRef]

28. Baird, R.; Eaton, A.D.; Rice, E.; Bridgewater, L. *American, Standard Methods for the Examination of Water and Wastewater*; Public Health Association: Washington, DC, USA, 2023.

29. Nekuri, B.B. Application of Iron Oxide Nanoparticles in the Dye Removal. *Int. J. Civ. Eng. Technol.* **2017**, *8*, 1243–1253.

30. Karimi, E.; Jeffryes, C.; Yazdian, F.; Akhavan Sepahi, A.; Hatamian, A.; Rasekh, B.; Ashrafi, S.J. DBT Desulfurization by Decorating Rhodococcus Erythropolis IGTS8 Using Magnetic Fe_3O_4 Nanoparticles in a Bioreactor. *Eng. Life Sci.* **2017**, *17*, 528–535. [CrossRef]

31. Yan, H.; Zhang, J.; You, C.; Song, Z.; Yu, B.; Shen, Y. Influences of Different Synthesis Conditions on Properties of Fe_3O_4 Nanoparticles. *Mater. Chem. Phys.* **2009**, *113*, 46–52. [CrossRef]

32. Ali, A.; Chiang, Y.W.; Santos, R.M. X-ray Diffraction Techniques for Mineral Characterization: A Review for Engineers of the Fundamentals, Applications, and Research Directions. *Minerals* **2022**, *12*, 205. [CrossRef]

33. Khan, U.S.; Amanullah; Manan, A.; Khan, N.; Mahmood, A.; Rahim, A. Transformation Mechanism of Magnetite Nanoparticles. *Mater. Sci. Pol.* **2015**, *33*, 278–285. [CrossRef]

34. Pereira, M.J.; Carvalho, E.; Eriksson, J.W.; Crans, D.C.; Aureliano, M. Effects of Decavanadate and Insulin Enhancing Vanadium Compounds on Glucose Uptake in Isolated Rat Adipocytes. *J. Inorg. Biochem.* **2009**, *103*, 1687–1692. [CrossRef]

35. Flood-Garibay, J.A.; Méndez-Rojas, M.A. Synthesis and Characterization of Magnetic Wrinkled Mesoporous Silica Nanocomposites Containing Fe_3O_4 or $CoFe_2O_4$ Nanoparticles for Potential Biomedical Applications. *Colloids Surf. A Physicochem. Eng. Asp.* **2021**, *615*, 126236. [CrossRef]

36. Li, G.Y.; Jiang, Y.R.; Huang, K.L.; Ding, P.; Chen, J. Preparation and Properties of Magnetic Fe_3O_4–Chitosan Nanoparticles. *J. Alloy. Compd.* **2008**, *466*, 451–456. [CrossRef]

37. Nigam, S.; Barick, K.C.; Bahadur, D. Development of Citrate-Stabilized Fe_3O_4 Nanoparticles: Conjugation and Release of Doxorubicin for Therapeutic Applications. *J. Magn. Magn. Mater.* **2011**, *323*, 237–243. [CrossRef]

38. Frost, R.L.; Weier, M.L.; Kloprogge, J.T. Raman Spectroscopy of Some Natural Hydrotalcites with Sulphate and Carbonate in the Interlayer. *J. Raman Spectrosc.* **2003**, *34*, 760–768. [CrossRef]

39. Innocenzi, P.; Falcaro, P.; Grosso, D.; Babonneau, F. Order−Disorder Transitions and Evolution of Silica Structure in Self-Assembled Mesostructured Silica Films Studied through FTIR Spectroscopy. *J. Phys. Chem. B* **2003**, *107*, 4711–4717. [CrossRef]

40. Ma, M.; Zhang, Y.; Yu, W.; Shen, H.Y.; Zhang, H.Q.; Gu, N. Preparation and Characterization of Magnetite Nanoparticles Coated by Amino Silane. *Colloids Surf. A Physicochem. Eng. Asp.* **2003**, *212*, 219–226. [CrossRef]

41. Waldron, R.D. Infrared Spectra of Ferrites. *Phys. Rev.* **1995**, *99*, 1727. [CrossRef]

42. Gasparov, L.V.; Tanner, D.B.; Romero, D.B.; Berger, H.; Margaritondo, G.; Forro, L. Infrared and Raman Studies of the Verwey Transition in Magnetite. *Phys. Rev. B* **2000**, *62*, 7939. [CrossRef]
43. Maharaj, D.; Bhushan, B. Effect of Spherical Au Nanoparticles on Nanofriction and Wear Reduction in Dry and Liquid Environments. *Beilstein J. Nanotechnol.* **2012**, *3*, 759–772. [CrossRef]
44. Palchoudhury, S.; Baalousha, M.; Lead, J.R. Methods for Measuring Concentration (Mass, Surface Area and Number) of Nanomaterials. *Front. Nanosci.* **2015**, *8*, 153–181. [CrossRef]
45. Saleh, T.A. Isotherm Models of Adsorption Processes on Adsorbents and Nanoadsorbents. *Interface Sci. Technol.* **2022**, *34*, 99–126. [CrossRef]
46. Mahmoud, A.S.; Farag, R.S.; Elshfai, M.M. Reduction of Organic Matter from Municipal Wastewater at Low Cost Using Green Synthesis Nano Iron Extracted from Black Tea: Artificial Intelligence with Regression Analysis. *Egypt. J. Pet.* **2019**, *29*, 9–20. [CrossRef]
47. Saryel-Deen, R.A.; Mahmoud, A.S.; Mahmoud, M.; Mostafa, M.K.; Peters, R.W. Adsorption and Kinetic Studies of Using Entrapped Sewage Sludge Ash in the Removal of Chemical Oxygen Demand from Domestic Wastewater, with Artificial Intelligence Approach. In Proceedings of the 2017 Annual AIChE Meeting, Minneapolis, MN, USA, 29 October–3 November 2017.
48. Farag, R.S.; Elshfai, M.M.; Mahmoud, A.S.; Mostafa, M.K.; Karam, A.; Peters, R.W. (670d) Study the Degradation and Adsorption Processes of Organic Matters from Domestic Wastewater Using Chemically Prepared and Green Synthesized Nano Zero-Valent Iron. In Proceedings of the AIChE Annual Meeting 2019, Orlando, FL, USA, 10–15 November 2019.
49. Nassar, N.N.; Arar, L.A.; Marei, N.N.; Ghanim, M.M.A.; Dwekat, M.S.; Sawalha, S.H. Treatment of Olive Mill Based Wastewater by Means of Magnetic Nanoparticles: Decolourization, Dephenolization and COD Removal. *Environ. Nanotechnol. Monit. Manag.* **2014**, *1*, 14–23. [CrossRef]
50. Soliman, N.K.; Moustafa, A.F. Industrial Solid Waste for Heavy Metals Adsorption Features and Challenges; a Review. *J. Mater. Res. Technol.* **2020**, *9*, 10235–10253. [CrossRef]
51. Umoren, S.A.; Etim, U.J.; Israel, A.U. Adsorption of Methylene Blue from Industrial Effluent Using Poly (Vinyl Alcohol). *J. Mater. Environ. Sci.* **2013**, *4*, 75–86.
52. Sahu, O.P.; Chaudhari, P.K. Review on Chemical Treatment of Industrial Waste Water. *J. Appl. Sci. Environ. Manag.* **2013**, *17*, 241–257. [CrossRef]
53. Zhou, Y.; Liang, Z.; Wang, Y. Decolorization and COD Removal of Secondary Yeast Wastewater Effluents by Coagulation Using Aluminum Sulfate. *Desalination* **2008**, *225*, 301–311. [CrossRef]
54. Cao, M.; Li, Z.; Wang, J.; Ge, W.; Yue, T.; Li, R.; William, W.Y. Food Related Applications of Magnetic Iron Oxide Nanoparticles: Enzyme Immobilization, Protein Purification, and Food Analysis. *Trends Food Sci. Technol.* **2012**, *27*, 47–56. [CrossRef]
55. Phouthavong, V.; Yan, R.; Nijpanich, S.; Hagio, T.; Ichino, R.; Kong, L.; Li, L. Magnetic Adsorbents for Wastewater Treatment: Advancements in Their Synthesis Methods. *Materials* **2022**, *15*, 1053. [CrossRef]
56. Nguyen, M.D.; Tran, H.V.; Xu, S.; Lee, T.R. Fe_3O_4 Nanoparticles: Structures, Synthesis, Magnetic Properties, Surface Functionalization, and Emerging Applications. *Appl. Sci.* **2021**, *11*, 11301. [CrossRef] [PubMed]
57. Barnwell, F.H.; Brown, F.A. Responses of Planarians and Snails. In *Biological Effects of Magnetic Fields*; Barnothy, M.F., Ed.; Springer US: Boston, MA, USA, 1964; pp. 263–278. [CrossRef]
58. Tomska, A.; Wolny, L. Enhancement of Biological Wastewater Treatment by Magnetic Field Exposure. *Desalination* **2008**, *222*, 368–373. [CrossRef]